Highlights

Optical tool deflection measurement approach using shadow imaging

Marina Terlau, Axel von Freyberg, Dirk Stöbener, Andreas Fischer

- Multi-sensor system is designed for tool deflection measurement.
- Model-based calibration procedure is introduced.
- Shadow imaging sensor is investigated for lateral and axial position measurement.
- Random and systematic position measurement error is characterized.

Optical tool deflection measurement approach using shadow imaging

Marina Terlau[a,*], Axel von Freyberg[a], Dirk Stöbener[a,b], Andreas Fischer[a,b]

[a] *University of Bremen, Bremen Institute for Metrology, Automation and Quality Science, Linzer Straße 13, D-28359 Bremen, Germany*
[b] *MAPEX Center for Materials and Processes, University of Bremen, P.O. box 330440, D-28334 Bremen, Germany*

Abstract

In incremental sheet forming, geometrical deviations occur due to deflections of the forming stylus. To compensate the deviations, a non-contact in-process tool deflection measurement is required that is capable of measuring the tool tip position with a measurement uncertainty of 15 µm in a volume of 2.0 m × 1.0 m × 0.2 m. For this purpose, an optical multi-sensor system is designed. Each sensor evaluates the lateral shift and the magnification of the shadow cast from the LED attached to the tool tip, to enable measuring the lateral and axial tool tip position component, respectively. The experimental validation shows that the sensing principle is sufficiently robust regarding ambient light. As a result, despite a remaining systematic error after calibration that dominates the uncertainty, the measurement requirements are fulfilled by a single sensor regarding the lateral position component. For the axial position component, a triangulation with two sensors is necessary.

Keywords: incremental sheet forming, multiple sensing, shadow imaging

1. Introduction

1.1. Motivation

For the manufacture of large sheet metal parts in small batches, incremental sheet forming (ISF) is an economical alternative to conventional forming processes [1]. The main disadvantage of forming processes like deep drawing for the manufacture of small batches is the cost-intensive and time-consuming production and modification of the required tools. In contrast to conventional forming processes, ISF uses a universal forming stylus that forms the sheet metal step by step over a counter die [2]. Since the counter die can be 3D-printed, the production of the first part is less cost-intensive and time-consuming. However, the main drawbacks of ISF are geometrical deviations caused by spring back [3] and deflections of the forming tool [4]. To enable a compensation of the tool deflection, the deflection must be determined. This is usually solved by predicting the tool deflection based on mechanical calculations [5]. However, the prediction is based on model assumptions and does not include the machine tool error or machine deformations. Therefore, a tool deflection measurement is required which is independent of these restrictions and, thus, provides the tool deflection with minimal uncertainty.

1.2. State of the art

The required measurement system must be capable of measuring the tool deflection in-process close to the tool contact point. Furthermore, the measurement should be contactless and independent of the machine tool kinematic. Therefore, potential measurement systems are narrowed down to optical systems.

For the considered application, the tool deflection measurement during ISF, a machining volume of 2.0 m × 1.0 m × 0.2 m has to be covered. Assuming typical tool deflections between 150 µm and 450 µm [5], a position measurement uncertainty of 15 µm is demanded, according to the golden rule of measurements. This means a challenging dynamic range > 10^5, which follows from the measurement range divided by the required uncertainty. A scanning measurement approach might be suitable to reach the necessary dynamic range. However, assuming a usual tool feed rate of 50 mm/s [6], the scan duration per measurement point should not exceed 300 µs to avoid motion blur, which is difficult to achieve.

Non-scanning measurement approaches are an alternative, which can be divided into global and local approaches. With a global measurement approach, like full-field photogrammetry, the full field is captured with a single shot but the required dynamic range is not reachable [7]. The measurement range of a locally measuring system can be enlarged by tracking the point of interest. Laser trackers, for instance, form a common system to measure the machine tool error [8]. Tracking systems contain a position control system to enable an active movement of the measuring system to follow the point of interest. But, if the view is lost and the point of interest gets outside the system's field of view, the measurement will fail. The moving parts enabling an active sensor movement, the position control system and the probability of failure due to a loss of view limit

Abbreviations: CMM, coordinate measuring machine; CNR, contrast-to-noise ratio; ISF, incremental sheet forming; MCS, machine coordinate system; SCS, sensor coordinate system

*Corresponding author

Email addresses: m.terlau@bimaq.de, 0000-0002-5698-7049 (Marina Terlau), a.freyberg@bimaq.de, 0000-0002-0936-3655 (Axel von Freyberg), d.stoebener@bimaq.de, 0000-0002-1624-2106 (Dirk Stöbener), andreas.fischer@bimaq.de, 0000-0001-7349-7722 (Andreas Fischer)

the robustness of tracking systems. In order to combine the low uncertainty of a local approach and the large measuring volume of a global approach, a multiple sensing approach is applied here. Thereby, the measurement system consists of several coupled sensors, each of them covering a sub-region of the measurement volume. As a result, the whole machining volume is continuously covered by multiple smaller and overlapping measurement areas without the need for an active tracking, i. e. no moving parts.

For tool deflection measurement with the chosen multiple sensing approach, at least 20 sensors are arranged outside the machine tool area on a separate frame, all at the same height, in the middle of the 200 mm high machining volume. A possible sensor arrangement for a section of the machining volume is depicted in Fig. 1. As a result of this sensor arrangement, each sensor has to provide an axial measurement range of at least 500 mm. The required lateral measurement range depends on the number of sensors used. Note that the main tool deflection component occurs in horizontal direction, i. e. in the (x, y)-plane of the machine coordinate system [5]. For this reason, the tool deflection component in the vertical direction, i. e. in z-direction, is not considered further.

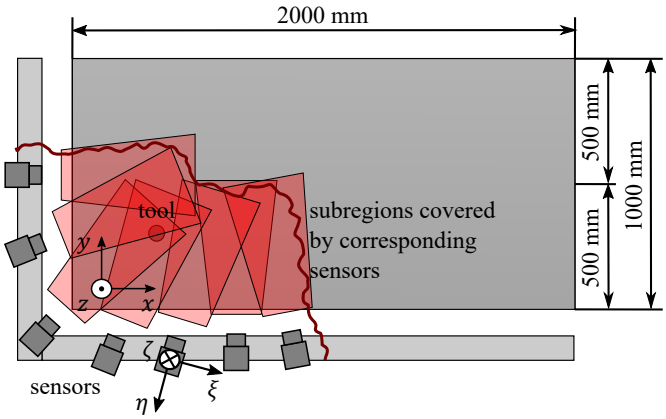

Figure 1: Section of a multi-sensor-setup for tool deflection measurement. Each sensor covers a sub-region of the measurement volume. Some sensors and their sub-regions, which are highlighted in light red, are arranged as examples. Additional sensors are needed to cover the entire machining volume.

Each sensor of the multi-sensor system must be able to measure the tool tip displacement in both the axial and the lateral direction from the sensor perspective. Optical measurement principles for axial displacement measurement are classified by Berkovic and Shafir [9] in intensity-based sensors, triangulation sensors, time-of-flight sensors, confocal sensors and interferometric sensors. The working distance of intensity-based sensors and confocal sensors is located too close for the proposed application and the range of time-of-flight sensors is located too far. Considering interferometric sensors, the working distance fits the requirements, and using digital holography, a lateral displacement can also be measured. Although digital holography increases the lateral measurement range of interferometric sensors, a lateral measurement range of 20 mm [10] is still too small. The class of triangulation sensors includes, on the one hand, systems in which light is emitted at one point and the scattered light from the surface is detected at another point so that only one detector is used. This category of triangulation systems contains 1D laser triangulation sensors, the light section method and fringe projection. On the other hand, there are triangulation-based systems that use two detectors, which measure either the angle of view or the distance to a marked point from two known observation points. Applying the angle-of-view measurement method, the required axial and lateral measurement range is realizable and a three-dimensional position measurement is possible without the need of combining several techniques but by using a single principle.

Photogrammetry is a common method for angle-of-view triangulation measurements. Regarding the aimed optical tool deflection measurement, the point of interest, the tool tip, represents only a small section in the imaged field of view. Even if the tool tip is highlighted by a colorful patterned print or an attached light source, the amount of features in the camera image will be low. Consequently, the measurement uncertainty is relatively high [11]. Coded-aperture imaging represents an alternative method to conventional imaging. In coded-aperture imaging, a coded mask is positioned in front of the camera chip instead of a lens. This setup allows both measuring the angle and the depth of the imaged 3D scene by only one camera [12]. Zhuo et al. showed an error of 0.22 % of the maximum working distance for the depth estimation by means of a simulation [13]. Furthermore, coded-aperture imaging performs best if the field of view contains only one point light source [14]. The single light source, that can be attached to the tool tip, casts a shadow through the coded mask onto the camera chip, which is why the coded-aperture principle using one light source is also called shadow imaging [15]. In contrast to conventional imaging, the information is spread over the camera image and not concentrated on a few pixels, which enables averaging in order to minimize the measurement uncertainty. Therefore, shadow imaging is selected for tool deflection measurement. An evaluation of the shadow shift allows to calculate the lateral shift of the light source, and the axial distance can be calculated based on the magnification of the projected image of the mask with respect to the mask [16].

At present, there are various measurement systems that are based on shadow imaging. Iafolla et al. [17] positioned the light source onto the shadow mask, implemented a mirror that reflected the light back to the sensor, and then measured the angle of the mirror. Other systems measure the shift of a patterned mask, that moves with respect to sensor and light source [18, 19]. As the position and not the angle of the tool tip is of interest, the concept of Iafolla et al. is not pursued further. Approaches which measure the mask shift are not appropriate for tool deflection measurement, since a mask, that is large enough, can not be attached to the tool and a fixed sensor position is demanded for the sake of robustness. Therefore, for the application in ISF, the elementary sensor setup without moving parts is used.

A periodic grated mask leads to an ambiguous displacement measurement that is limited to one lateral measurement dimension. Both challenges are also present in systems that do not

utilize shadow imaging but measure the lateral shift of a black and white pattern. While Fu et al. [20] measure a relative one-dimensional displacement using a periodic grated pattern, André et al. [21] implemented a two-dimensional pattern with absolute coding elements, that allows a two-dimensional absolute shift measurement. Different image evaluation algorithms are available to calculate the shift of the pattern in the captured image. If the pattern contains periodic elements, the phase shift can be used to determine the shift of the imaged pattern [18, 21]. Furthermore, a correlation algorithm is applicable for pattern shift calculation in images [17], and Yu et al. implemented a quadratic fitting to localize the grating [19]. Since shadow imaging is based on a shift measurement in camera images, the standard uncertainty of the pattern shift in the image plane serves as a quality measure for the systems' measurement capability. Previous investigations show a shift standard uncertainty in the image plane of $\frac{1.5}{1000}$ px [17] to $\frac{4.9}{1000}$ px [18]. Both results demonstrate the sub-pixel resolution capability, which highlights the potential of the shadow imaging principle.

In summary, shadow imaging forms a promising technique for the lateral displacement measurement of the tool tip during ISF. However, it needs to be clarified whether the position measurement uncertainty meets the requirement for the tool deflection measurement in the required measuring volume. The same applies to the axial position measurement. Indeed, a higher uncertainty is expected for the axial position measurement due to the small sensor aperture. The question therefore is, whether a single sensor is sufficient or a triangulation with a second sensor is necessary to fulfill the uncertainty requirement regarding the axial position. Finally, the influence of ambient light is an additional highly relevant uncertainty source with respect to the sensor's application in ISF. Therefore, the influence of ambient light must be characterized in addition to the influence of image noise.

1.3. Aim and outline

The aim of this work is to assess the random and systematic position measurement errors of a single shadow imaging sensor with respect to its potential application in a multi-sensor system to measure the tool deflection during ISF. For this purpose, the achievable dynamic range of a single sensor is investigated in both lateral and axial direction. Furthermore, this study considers the influence of the measuring environment, i. e. the illumination in a manufacturing environment.

Section 2 introduces the principle of measurement in detail. Section 3 describes the experimental setup and its modification to study the influence of environmental illumination on the uncertainty. The results focussing on systematic errors, which remain after a proposed calibration procedure, and on random errors are presented and discussed in section 4. Finally, section 5 provides a conclusion and an outlook.

2. Principle of measurement

The proposed shadow imaging sensor, which is intended to be applied in a multiple sensing system for tool deflection measurement, is built up from a mask that has transparent and opaque features and a camera that is located behind the mask, see Fig. 2. The light source to be located is fixed on the tool near the tool contact point. The measurement of the vertical component z_L of the light source position is not addressed in this work, because the main tool deflection occurs in the horizontal plane. The position components x_L and y_L are measured by evaluating different shadow features, while both approaches rely on the triangulation principle. For the intended assessment of the measurement capability regarding each position component, the measurement of x_L and y_L are studied separately. For this purpose, the ideal condition is assumed that, for the measurement of x_L, the component y_L is known with negligible uncertainty and vice versa.

The light source position component x_L describes the lateral position component (for small sensor angles γ around z-axis of the machine coordinate system (MCS)). From the detected angle Θ_M to the light source in the MCS, the sensor position $(x_\mathrm{S}, y_\mathrm{S})$ and the position component y_L of the light source, the lateral position component is calculated by

$$x_\mathrm{L} = x_\mathrm{S} + (y_\mathrm{L} - y_\mathrm{S}) \cdot \tan(\Theta_\mathrm{M}). \tag{1}$$

The angle in the MCS

$$\Theta_\mathrm{M} = \Theta_\mathrm{S} - \gamma \tag{2}$$

is determined from the angle Θ_S that the sensor measures and the calibrated orientation γ of the (ξ, η, ζ) sensor coordinate system (SCS) the MCS. The sensor orientation in the two other directions can be neglected, because a rotation around the x-axis has no influence on the angle Θ_M and the rotation angle around the y-axis is negligible with proper sensor adjustment as it affects the angle Θ_M with its cosine. The light source projects a point of the mask to the camera so that the associated shadow appears in the (ξ, ζ) image plane. The shadow position ξ_i in the camera image, where the shadow of a defined line in the mask occurs, and the distance h_2 between the camera and the mask provide the angle

$$\Theta_\mathrm{S} = \arctan\left(\frac{\xi_{\mathrm{i},0} - \xi_\mathrm{i}}{h_2}\right) \tag{3}$$

wherein $\xi_{\mathrm{i},0}$ is the shadow position associated to a light source position centrally in front of the sensor. Image processing of the recorded images is used to extract the shadow position.

The light source position component y_L is mainly the axial measurement distance, because the y-axis is oriented approximately axially to the sensor's viewing direction. It follows from the sensor position $(x_\mathrm{S}, y_\mathrm{S})$, the position component x_L, the sensor's orientation γ in the MCS and the axial distance h_1 (to be measured) from the sensor to the LED:

$$y_\mathrm{L} = y_\mathrm{S} + \frac{h_1}{\cos(\gamma)} + (x_\mathrm{L} - x_\mathrm{S}) \cdot \tan(\gamma). \tag{4}$$

Depending on the axial distance to the light source, the mask pattern is magnified by shadow projection. Thus, the magnification of a characteristic feature length l_M of the mask to the

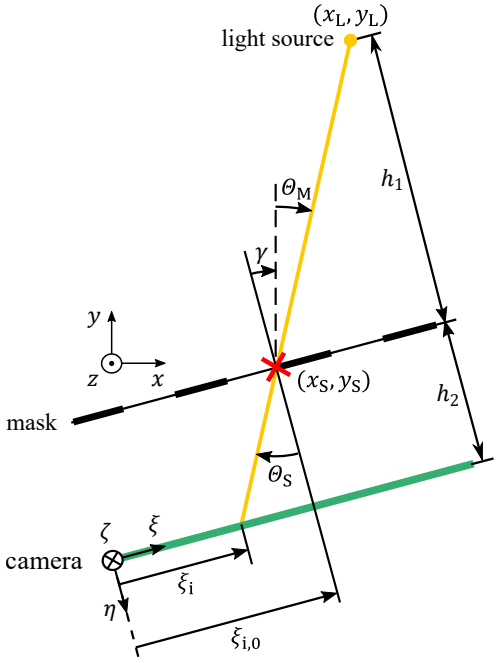

Figure 2: Principle of the angle measurement with the shadow imaging sensor. The light source at position (x_L, y_L) in the machine coordinate system (x, y, z) casts a shadow through the mask that appears at the shadow position ξ_i in the sensor coordinate system (ξ, η, ζ).

associated length l_S in the projected image provides the axial distance

$$h_1 = \frac{l_M \cdot h_2}{l_S - l_M}. \tag{5}$$

While the length l_M of a selected characteristic feature is known or calibrated, the corresponding length l_S is extracted from the camera image.

As a result of the equation systems (1)-(3) and (4)-(5), respectively, both components of the light source position are calculated based on camera image features. For this purpose, the sensor position (x_S, y_S) and orientation γ, the distance h_2 between mask and camera and the characteristic length l_M of the mask need to be calibrated.

3. Methods

3.1. Experimental setup

In the conducted experiments, the sensor consist of a monochrome camera and a mask with a vertical stripe pattern. The camera is a DMM 37UX273-ML monochrome board camera from the company The Imaging Source, which has a 1440 × 1080 px² CMOS image sensor, whose pixels are quadratic with 3.45 µm edge length. The mask pattern contains 80 µm wide transparent stripes and opaque stripes, most of which are 170 µm, but every fifth stripe is 181 µm wide which enlarges the unambiguous measurement range. The distance h_2 between the camera and the mask is set to approximately 20 mm. The light source is an SMD-LED with a peak wavelength of 518 nm and an luminous intensity between 180 mcd and 450 mcd. Based on the basic components, camera, mask and LED, two experimental setups are realized to conduct different measuring programs.

In the first experimental setup shown in Fig. 3, a positioning unit moves the LED in lateral direction only, i. e. parallel to the camera chip. The constant axial distance h_1 between the mask and the LED is approximately 230 mm. The LED shift is recorded by a laser interferometer as a reference, which actually measures the shift of a mirror to which the LED is attached. The positioning unit moves the LED step-by-step to 300 positions with a step size of 200 µm. At each position, the camera captures one image with an exposure time of 10 ms. The experiment is performed to first investigate the sensor's capability to measure the angle Θ_M to a light source as an important intermediate quantity for determining x_L, while the axial distance variations, that complicate the evaluation procedure due to a position depending magnification of the recorded shadow, are excluded in this experimental setup.

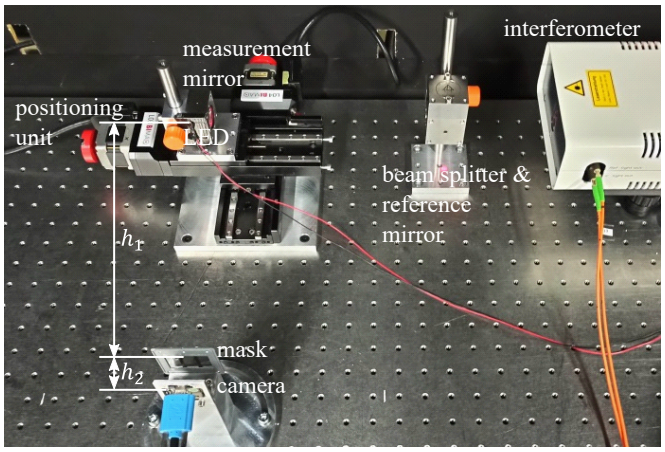

Figure 3: Experimental setup for investigating the sensor's capability of the lateral position measurement. The lateral LED shift leads to a shadow shift to be evaluated in different ambient illuminations.

Furthermore, the setup is extended to test two different illumination conditions. For the realization of an ideal illumination condition, a dark box surrounds the setup to avoid the influence of environmental light. To emulate the illumination condition in a common manufacturing environment, the dark box is removed and, in addition to the laboratory lighting, an LED spotlight is positioned above the setup to adjust the brightness of the disturbing light. The illuminance is set to > 200 lux which is required for manufacturing environments, according to labor law regulations. The conduction of the experiment in both illumination conditions enable an experimental investigation of the influence of environmental illumination.

In the second setup, a coordinate measuring machine (CMM) is used to move the attached LED through the field of view of the sensor as shown in Fig. 4. The reference position $(x_{L,ref}, y_{L,ref})$ is measured by the CMM simultaneously. The LED positions, shown in Fig. 4 b), are arranged row-wise, where 31 positions are defined per row with an equal y-coordinate, i. e. an equal distance to the sensor. 65 rows are located at various distances ranging from 100 mm to 600 mm

wherein the rows are closer to each other the closer the row is to the sensor. The positions in each row are equally distributed and span an angle of view from -4.3° to +4.3°. To prevent the experiment from interfering ambient light, the experimental setup operates in a dark laboratory.

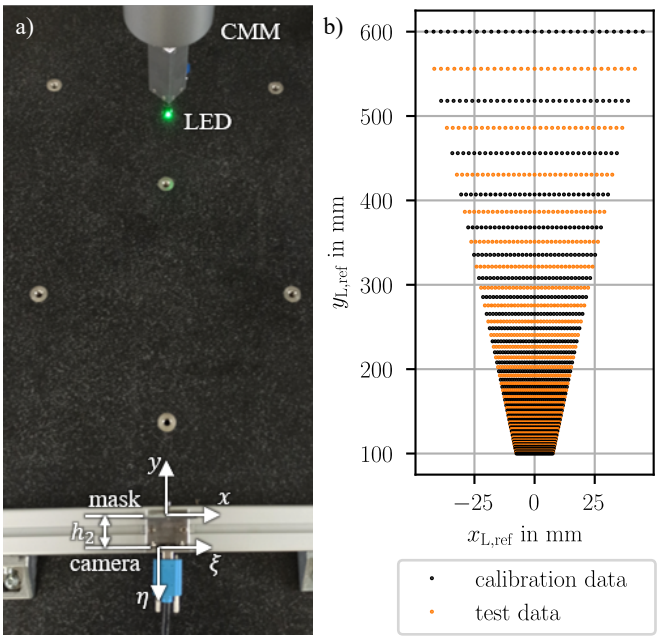

Figure 4: Experimental setup for investigating the sensor's capability of lateral and axial position measurement in a two-dimensional measuring area: a) setup of the experiment using a CMM to move the LED; b) specified LED positions of both the calibration and test data set to explore the sensor's position measurement capability.

The CMM-setup is used to finally investigate the validity of the measurement system in the studied two-dimensional measuring area for the measurement of the lateral LED position x_L and of the axial LED position y_L. At each LED position, 10 images are captured with an exposure time of 10 ms. Several camera images at each position enable the assessment of random and systematic position error components. Furthermore, the field of data is divided into two datasets for calibrating and testing. Thereby, every second row is used for calibration and the remaining rows for testing.

3.2. Image processing

For measuring the lateral position component x_L according to Eq. (1)-(3), the shadow position ξ_i must be detected in the captured camera images. Here, it is sufficient to define a certain shadow position as the starting position and then detect the shadow shifts. The magnification, i. e. the length l_S of a feature in the shadow, which is required for measuring the axial position component y_L according to Eq. (4)-(5), can be determined by evaluating the stripe spacing of the shadow.

Several image processing methods are applicable to evaluate the shadow position as well as the stripe spacing. Preliminary tests have shown that the approximation of each intensity maximum by a model function is the most suitable procedure to extract the shadow position and is additionally capable of detecting the stripe spacing, varied by the magnification [22]. Another advantage of the model function approximation is that shadows of aperiodic patterned masks, which extend the unambiguous measurement range, can be evaluated in the same way as shadows of periodic patterned masks.

To implement the approximation, the data is preprocessed first. Column-wise averaging is the first step to reduce image noise and artifacts. Subsequently, a low-pass filter smoothens the averaged intensity curve. To separate each white stripe to be approximated, partitioning of the camera image is performed at the local intensity minima of the dark stripes. Subsequently, a limited Gaussian function is approximated to the intensity profile of each individual white stripe. The applied model function

$$I_M(\xi) = \begin{cases} I_0 + A \cdot e^{-\left(\frac{|\xi-\mu|}{w}\right)^2} & \text{for } I(\xi) < I_{max} \\ I_{max} & \text{for } I(\xi) \geq I_{max} \end{cases}, \tag{6}$$

is modified by the offset I_0 (the intensity minimum), the amplitude of the curve A, i. e. the difference between intensity maximum and minimum, the peak position μ within the partition, the width w of the Gaussian intensity distribution and the limitation value I_{max} that restricts the maximum intensity and creates a flat top. With approximated modification parameters, the model function corresponds to the curve of the intensity profile. Since the parameter μ represents the peak ξ-position, a location can be assigned to each white stripe.

If the axial distance to the sensor does not vary, i. e. the stripe spacing is constant in the projected images of the mask, the stripe shifts can be calculated from two subsequent camera images and the averaged stripe shift describes the shadow shift. The cumulated shadow shifts give the shadow position from which the lateral LED position x_L is calculated. After approximation of the model function, the stripe spacing is calculated easily from the individual stripe positions as well and consequently provides the axial position component y_L according to Eq. (4)-(5).

For the examination of the two-dimensional measurement area, the distance between sensor and light source varies so that the stripe shift is not equal for all stripes in the camera images. For this reason, the shadow position evaluation is extended to enable measuring the lateral position x_L even at varying distances. Therefore, the position ξ_i of a reference stripe, is evaluated and tracked. In order to include the information of all stripe positions available in one camera image, the magnification

$$k = \frac{l_S}{l_{S,0}} \tag{7}$$

of the present stripe spacing l_S with respect to the spacing $l_{S,0}$ for a reference light source distance is calculated for each camera image first. Then, the stripe spacing, extracted from each camera image, is scaled to the reference light source distance. The scaled stripe spacings are cumulated to determine the total spacing from each stripe to the reference stripe. The total spacings are calibrated by averaging over all camera images in the calibration data. The calibrated spacings form a reference table

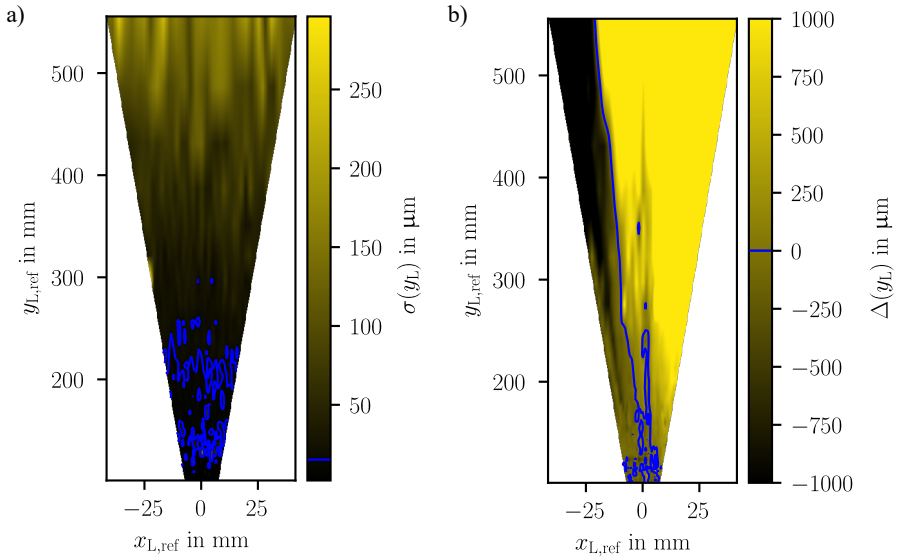

Figure 12: Error of the calculated axial position y_L of the LED interpolated between the LED positions from the test data. a) Random position error $\sigma(y_L)$ calculated by the standard deviation; b) systematic position error $\Delta(y_L)$ given by the deviation of the averaged evaluated axial position from the reference axial position.

Conflict of interest

The authors declare that they have no known competing financial interests or personal relationships that could have appeared to influence the work reported in this paper.

Acknowledgement

The IGF project No. 290 EBG of the Research Association for Measurement, Control and Systems Engineering (DFMRS) has been funded via the AiF within the transnational CORNET program by the Federal Ministry of Economics and Climate Protection based on an enactment of the German Parliament.

References

[1] A. Kumar, V. Gulati, Experimental investigations and optimization of forming force in incremental sheet forming, Sādhanā 43 (10) (2018) 42. doi:10.1007/s12046-018-0926-7.

[2] N. Devarajan, G. Sivaswamy, R. Bhattacharya, D. P. Heck, M. A. Siddiq, Complex incremental sheet forming using back die support on aluminium 2024, 5083 and 7075 alloys, Procedia Engineering 81 (2014) 2298–2304. doi:10.1016/j.proeng.2014.10.324.

[3] H. Ren, J. Xie, S. Liao, D. Leem, K. Ehmann, J. Cao, In-situ springback compensation in incremental sheet forming, CIRP Annals 68 (1) (2019) 317–320. doi:10.1016/j.cirp.2019.04.042.

[4] P. Konka, R. Lingam, U. A. Singh, C. Shivaprasad, N. V. Reddy, Enhancement of accuracy in double sided incremental forming by compensating tool path for machine tool errors, The International Journal of Advanced Manufacturing Technology 111 (3-4) (2020) 1187–1199. doi:10.1007/s00170-020-06149-1.

[5] P. Konka, R. Lingam, N. V. Reddy, Tool path design system to enhance accuracy during double sided incremental forming - an analytical model to predict compensations for small/large components, Journal of Manufacturing Processes 58 (2020) 510–523.

[6] A. Kumar, V. Gulati, P. Kumar, Investigation of process variables on forming forces in incremental sheet forming, International Journal of Engineering and Technology 10 (3) (2018) 680–684. doi:10.21817/ijet/2018/v10i3/181003021.

[7] D. Sims-Waterhouse, M. Isa, S. Piano, R. Leach, Uncertainty model for a traceable stereo-photogrammetry system, Precision Engineering 63 (2020) 1–9. doi:10.1016/j.precisioneng.2019.12.008.

[8] U. Mutilba, J. A. Yagüe-Fabra, E. Gomez-Acedo, G. Kortaberria, A. Olarra, Integrated multilateration for machine tool automatic verification, CIRP Annals 67 (1) (2018) 555–558. doi:10.1016/j.cirp.2018.04.008.

[9] G. Berkovic, E. Shafir, Optical methods for distance and displacement measurements, Advances in Optics and Photonics 4 (4) (2012) 441–471. doi:10.1364/AOP.4.000441.

[10] J. Dong, S. Jia, C. Jiang, Surface shape measurement by multi-illumination lensless fourier transform digital holographic interferometry, Optics Communications 402 (2017) 91–96. doi:10.1016/j.optcom.2017.05.051.

[11] F. Dai, Y. Feng, R. Hough, Photogrammetric error sources and impacts on modeling and surveying in construction engineering applications, Visualization in Engineering 2 (1) (2014).

[12] A. Levin, R. Fergus, F. Durand, W. T. Freeman, Image and depth from a conventional camera with a coded aperture, ACM Transactions on Graphics 26 (99) (2007) 70. doi:10.1145/1239451.1239521.

[13] C. Zhou, S. Lin, S. K. Nayar, Coded aperture pairs for depth from defocus and defocus deblurring, International Journal of Computer Vision 93 (1) (2011) 53–72. doi:10.1007/s11263-010-0409-8.

[14] K. D. Ridley, G. D. de Villiers, D. A. Payne, R. A. Wilson, C. W. Slinger, Visible band lens-free imaging using coded aperture techniques, in: S. Rogers, D. P. Casasent, J. J. Dolne, T. J. Karr, V. L. Gamiz (Eds.), Adaptive coded aperture imaging, non-imaging, and unconventional imaging sensor systems, SPIE Proceedings, SPIE, 2009, p. 746809. doi:10.1117/12.828580.

[15] P. Masa, E. Franzi, C. Urban, Nanometric resolution absolute position encoders, in: ESA (Ed.), Proceedings of 13th European Space Mechanisms and Tribology Symposium, 2009.

[16] E. Grenet, P. Masa, E. Franzi, D. Hasler, Measurement system of a light source in space (2015).

[17] L. Iafolla, L. Witthauer, A. Zam, G. Rauter, P. C. Cattin, Proof of principle of a novel angular sensor concept for tracking systems, Sensors and Actuators A: Physical 280 (2018) 390–398. doi:10.1016/j.sna.2018.08.012.

[18] V. Guelpa, G. J. Laurent, P. Sandoz, J. G. Zea, C. Clévy, Subpixelic measurement of large 1d displacements: principle, processing algorithms, performances and software, Sensors 14 (3) (2014) 5056–5073. doi:10.3390/s140305056.

[19] H. Yu, Q. Wan, Z. Mu, Y. Du, L. Liang, Novel nano-scale absolute linear displacement measurement based on grating projection imaging, Measurement 182 (2021) 109738. doi:10.1016/j.measurement.2021.109738.

[20] S. Fu, F. Cheng, T. Tjahjowidodo, M. Liu, Development of an image grating sensor for position measurement, Sensors 19 (22) (2019). doi:10.3390/s19224986.

[21] A. N. Andre, P. Sandoz, B. Mauze, M. Jacquot, G. J. Laurent, Sensing one nanometer over ten centimeters: A microencoded target for visual in-plane position measurement, IEEE/ASME Transactions on Mechatronics 25 (3) (2020) 1193–1201. doi:10.1109/TMECH.2020.2965211.

[22] M. Terlau, A. von Freyberg, D. Stöbener, A. Fischer, In-Prozess-Messung der Werkzeugablenkung beim inkrementellen Blechumformen, in: 21. GMA/ITG-Fachtagung: Sensoren und Messsysteme 2022, VDE Verlag GmbH Berlin Offenbach, 2022, pp. 90–96.